High frequency formulation for the acoustic power spectrum due to cascade-turbulence interaction

Cheolung Cheong
Acoustics and Vibration Group, Division of Physical Metrology, Korea Research Institute of Standards and Science, Daejeon 305-340, Korea

Phillip Joseph[a)]
Institute of Sound and Vibration Research, University of Southampton, Highfield, Southampton, SO17 1BJ, United Kingdom

Soogab Lee
Center for Environmental Noise and Vibration Research, School of Mechanical and Aerospace Engineering, Seoul National University, Seoul 151-742, Korea

(Received 14 April 2005; revised 1 September 2005; accepted 25 October 2005)

This paper investigates the noise radiated by a cascade of flat-plate airfoils interacting with homogeneous, isotropic turbulence. An analytic formulation for the spectrum of acoustic power of a two-dimensional flat-plate is derived. The main finding of this paper is that the acoustic power spectrum from the cascade of flat airfoils may be split into two distinct frequency regions of low frequency and high frequency, separated by a critical frequency. Below this frequency, cascade effects due to the interaction between neighboring airfoils are shown to be important. At frequencies above the critical frequency, cascade effects are shown to be relatively weak. In this frequency range, acoustic power is shown to be approximately proportional to the number of blades. Based on this finding at high frequencies, an approximate expression is derived for the power spectrum that is valid above the critical frequency and which is in excellent agreement with the exact expression for the broadband power spectrum. The formulation is used to perform a parametric study on the effects on the power spectrum of the blade number, stagger angle, gap-chord ratio, and Mach number. The theory is also shown to provide a close fit to the measured spectrum of rotor-stator interaction. © *2006 Acoustical Society of America.* [DOI: 10.1121/1.2139626]

PACS number(s): 43.28.Ra, 43.50.Cb [GCL] Pages: 108–122

I. INTRODUCTION

This paper deals with the broadband noise due to the interaction between turbulence and a cascade of flat-plate airfoils. This problem is relevant to broadband noise generation in an aero-engine due to interaction of the turbulent rotor wake with the stator vanes, and to the interaction of ingested turbulence with the rotor blades.

The acoustic radiation from a uniformly spaced cascade of blades due to an impinging turbulent gust may be predicted by Fourier synthesis of the response to a harmonic vortical gust. A number of different approaches have been developed to address this problem. Kaji and Okazaki[1,2] have considered sound propagation upstream through a two-dimensional cascade of flat-plate airfoils by solving for the distribution of dipole source strength on the blade surfaces. Based on a similar approach, Smith[3] has developed the first numerical solution for predicting the unsteady blade loading and the acoustic field upstream or downstream of a two-dimensional cascade of flat-plate airfoils perfectly aligned with a uniform mean flow. Further details are presented in Whitehead.[4] Mani and Hovray[5] have developed other methods for solving this problem using an approximate solution based on the Wiener Hopf method. Koch[6] extended the Wiener Hopf analysis of Mani and Hovray[5] to blades with finite chord and gave the transmission and reflection coefficient for both upstream and downstream propagating acoustic waves. Peake[7] has extended Koch's analysis to give the unsteady loading on the blades caused by an incoming vortical gust, and has also developed analytic tools[8,9] to enable the rapid computation of the function required for the Wiener Hopf solution. [5,6] The effects of blade sweep and oblique gust arrival angles were investigated by Glegg,[10] who has developed an analytic expression for the unsteady blade loading, acoustic mode amplitude, and sound power output of a three-dimensional rectilinear cascade of blades with finite chord excited by a three-dimensional vortical gust.

Hanson and Horan[11] have investigated the broadband noise due to turbulence interacting with a flat-plate cascade, using the cascade response theory due to Glegg.[10] Hanson[12,13] has also extended the theory in Ref. 11 to include the effects of lean and sweep on the broadband noise spectrum. Evers and Peake[14] have recently investigated the effects of small, but nonzero, camber and thickness on the upstream acoustic power.

In the present study, the theory of broadband noise from a cascade of two-dimensional flat airfoils subject to homogeneous frozen turbulent gust is investigated in detail. Emphasis is given to the physical interpretation of the acoustic field above a critical frequency, where it is shown that the sound

[a)]Electronic mail: pfj@isvr.soton.ac.uk

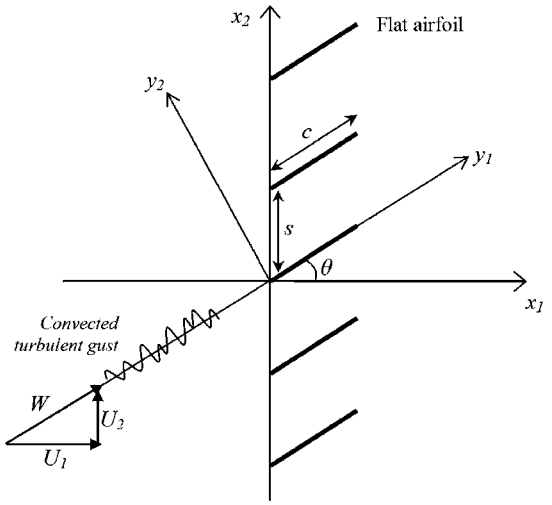

FIG. 1. The cascade geometry and the convected turbulence gust.

power is proportional to the blade number suggesting that for turbulent gusts, interaction effects between the blades is weak.

The main contributions of this paper are threefold. First, we define the concept of a critical frequency which divides the acoustic response of the flat-airfoil cascade to impinging turbulence into two distinct frequency regions. Below the critical frequency, the effects of interaction between the neighboring airfoils are significant and only some of the wave number components of turbulence contribute to the acoustic field. Above the critical frequency, all the wave number components of turbulence contribute to the acoustic field and the interaction between the adjacent airfoils is weak, so that the power from each blade is additive. Second, a simple expression is derived for the broadband power spectrum that is rapid to compute and is in excellent agreement with the exact calculation above the critical frequency. Finally, a parametric study is presented that includes a comparison between experimental data and predictions obtained using the exact and approximate expressions. This shows that overall predictions closely match those of Hanson[11,13] obtained using a three-dimensional theory, thereby suggesting that the contribution from oblique gusts to the radiated sound is comparatively weak.

II. FORMULATION OF ACOUSTIC FIELD

A. Basic equations

The cascade geometry and coordinate system investigated in this paper is shown in Fig. 1. A two-dimensional cascade of flat-plate airfoils with stagger angle θ is assumed to be located in a two-dimensional uniform flow moving in the direction parallel to the chord, i.e., with zero angle of incidence. Turbulence is assumed to be convected with the mean flow W as a "frozen gust pattern." In Fig. 1, (x_1,x_2) is the unwrapped duct coordinate system, and (y_1,y_2) is the cascade-fixed coordinate system. Following Smith, Ref. 3, nontrivial, single-frequency solutions of the linearized Euler equations of the form,

$$\begin{pmatrix} u_1 \\ u_2 \\ p \end{pmatrix} = \begin{pmatrix} \bar{u}_1 \\ \bar{u}_2 \\ \bar{p} \end{pmatrix} e^{i(\omega t+\alpha x_1+\beta x_2)}, \tag{1}$$

are obtained for

$$(\omega + U_1\alpha + U_2\beta)^2 - a^2(\alpha^2+\beta^2) = 0, \tag{2}$$

or

$$(\omega + U_1\alpha + U_2\beta) = 0, \tag{3}$$

where $\bar{u}$ and $\bar{p}$ are complex amplitudes, and α and β are the wave numbers of the perturbation quantities in the axial and gap-wise directions, respectively, and U_j is the mean velocity in the x_j direction, u_i is the unsteady velocity perturbation in the x_i direction, ρ_0 is the mean density, and p is the (acoustic) pressure. The dispersion relations of Eqs. (2) and (3) relate solely to acoustic waves and to vorticity waves, respectively. A single wave number component (k_1,k_2) of impinging turbulence has a phase angle σ between adjacent blades separated by a gap s given by

$$\sigma = (k_1 \sin\theta + k_2 \cos\theta)s. \tag{4}$$

The phase angle $\beta_r s$ between adjacent blades of the rth acoustic wave generated from the cascade due to a single wave number component of vorticity (k_1,k_2) is of the form $\beta_r s = \sigma - 2\pi r (r = -\infty, \ldots, -1, 0, 1, \ldots, \infty)$. The acoustic circumferential wave number β_r of the rth acoustic wave is therefore given by

$$\beta_r = \frac{(k_1 \sin\theta + k_2 \cos\theta)s - 2\pi r}{s}. \tag{5}$$

Equation (2) is a quadratic equation of the axial wave number α, whose solution can be expressed in terms of β_r and ω as follows:

$$\alpha_r^{\pm} = \frac{M_1(\omega/a + M_2\beta_r) \pm \sqrt{(\omega/a + M_2\beta_r)^2 - (1-M_1^2)\beta_r^2}}{1-M_1^2}. \tag{6}$$

The two solutions for α_r correspond to upstream-going (+) and downstream-going (−) acoustic waves. Note that β_r takes an infinite number of values, corresponding to an infinite number of cascade modes. However, Eq. (6) indicates that only a finite number of these can modes can propagate unattenuated. The amplitude of the cascade modes due to a harmonic gust can be obtained by following the procedure presented by Smith.[3] For a harmonic gust of the form,

$$w(y_1,y_2,t) = w_0 e^{i[k_1(y_1-Wt)+k_2 y_2]}, \tag{7}$$

the acoustic pressure upstream and downstream of the cascade (+,−) is of the form,

$$p^{\pm}(x_1,x_2,t) = \rho_0 W w_0 \sum_{r=-\infty}^{\infty} R_r^{\pm} e^{i(k_1 Wt + \alpha_r x_1 + \beta_r x_2)}, \tag{8}$$

where $R_r^{\pm}$ is the cascade response function, which is completely defined by the parameters of $s/c, \theta, M, \lambda$, and σ, where λ is the reduced frequency $\omega c/W$.

B. Acoustic power spectrum

The analysis of sound radiation due to an incident sinusoidal vortical gust can be extended to broadband turbulent velocity distributions via the Fourier transform. It is assumed here that the turbulence can be regarded as a "frozen gust pattern" convecting with the free stream velocity W. This is a reasonable assumption because turbulence velocities are generally much smaller than convection velocities and hence change only slightly as they are convected past any airfoil in the cascade. Equation (8) can be generalized to give the acoustic pressure radiated from a cascade subject to the impinging turbulent gust, in the form,

$$p^{\pm}(x_1,x_2,t) = \rho_0 W \int_{-\infty}^{\infty}\int_{-\infty}^{\infty} \hat{\hat{w}}(k_1,k_2) \sum_{r=-\infty}^{\infty} R_r^{\pm}(k_1,k_2) \times e^{i(k_1 Wt + \alpha_r^{\pm} x_1 + \beta_r x_2)} dk_1 dk_2, \tag{9}$$

where $\hat{\hat{w}}(k_1,k_2)$ is the two-dimensional wave number spectrum of the turbulence velocity evaluated in the moving reference frame. Taking the Fourier transform of Eq. (9) with respect to t gives

$$\tilde{p}_T^{\pm}(\mathbf{x},\omega) = \rho_0 \int_{-\infty}^{\infty} \hat{\hat{w}}(K_1,k_2) \sum_{r=-\infty}^{\infty} R_r^{\pm}(K_1,k_2) e^{i(\alpha_r^{\pm} x_1 + \beta_r x_2)} dk_2, \tag{10}$$

where $\tilde{p}_T^{\pm}(\mathbf{x},\omega) = (1/2\pi)\lim_{T\to\infty}\int_{-T}^{T} p^{\pm}(\mathbf{x},t) e^{-i\omega t} dt$ and $K_1 = \omega/W$. Equation (10) substituted into the linearized momentum equation gives the following expressions for the acoustic particle velocities in the axial and gap-wise directions, respectively,

$$\tilde{u}_{1,T}^{\pm}(\mathbf{x},\omega) = \rho_0 \int_{-\infty}^{\infty} \hat{\hat{w}}(K_1,k_2) \sum_{r=-\infty}^{\infty} \frac{-\alpha_r^{\pm} R_r^{\pm}(K_1,k_2) e^{i(\alpha_r^{\pm} x_1 + \beta_r x_2)}}{\rho_0(\omega + U_1\alpha_r^{\pm} + U_2\beta_r)} dk_2, \tag{11}$$

$$\tilde{u}_{2,T}^{\pm}(\mathbf{x},\omega) = \rho_0 \int_{-\infty}^{\infty} \hat{\hat{w}}(K_1,k_2) \sum_{r=-\infty}^{\infty} \frac{-\beta_r R_r^{\pm}(K_1,k_2) e^{i(\alpha_r^{\pm} x_1 + \beta_r x_2)}}{\rho_0(\omega + U_1\alpha_r^{\pm} + U_2\beta_r)} dk_2. \tag{12}$$

In a fluid moving at uniform velocity, the intensity spectrum is given by[15]

$$I^{\pm}(\omega) = \lim_{T\to\infty} \frac{\pi}{T} \mathrm{Re}\left\{ \left(\frac{\tilde{p}_T(\omega)}{\rho_0} + U_1 \tilde{u}_{1,T}^{\pm}(\omega) + U_2 \tilde{u}_{2,T}^{\pm}(\omega) \right) \times \left(\rho_0 \tilde{u}_{1,T}^{\pm *}(\omega) + \frac{U_1 \tilde{p}_T^{*}(\omega)}{a^2} \right) \right\}. \tag{13}$$

Inserting Eqs. (10)–(12) into Eq. (13), and treating w as a random variable, leads to

$$I^{\pm}(\mathbf{x},\omega) = \rho_0 \int_{-\infty}^{\infty}\int_{-\infty}^{\infty} \left[\begin{array}{l} \lim_{T\to\infty} \frac{\pi}{T} E[\hat{\hat{w}}(K_1,k_2)\hat{\hat{w}}^{*}(K_1,k_2')] \\ \sum_{r=-\infty}^{\infty}\sum_{r'=-\infty}^{\infty} \mathrm{Re}\left\{ \begin{array}{l} \dfrac{\omega(-\alpha_{r'}^{\pm *} + M_1(\omega/a + M_1\alpha_{r'}^{\pm *} + M_2\beta_{r'}))}{(\omega + U_1\alpha_r^{\pm} + U_2\beta_r)(\omega + U_1\alpha_{r'}^{\pm *} + U_2\beta_{r'})} \\ \times R_r^{\pm}(K_1,k_2) R_{r'}^{\pm *}(K_1,k_2) e^{i[(\alpha_r^{\pm} - \alpha_{r'}^{\pm *})x_1 + (\beta_r - \beta_{r'})x_2]} \end{array} \right\} \end{array} \right] dk_2 dk_2', \tag{14}$$

where E[ ] denotes the expected value, or ensemble average value. Assuming that $\hat{\hat{w}}$ is a statistically random variable, and that the velocities at different wave number are uncorrelated, Amiet[16] shows that

$$\lim_{T\to\infty} \frac{\pi}{T} E[\hat{\hat{w}}(K_1,k_2)\hat{\hat{w}}^{*}(K_1,k_2')] = W\delta(k_2 - k_2')\Phi_{ww}(K_1,k_2'), \tag{15}$$

where $\Phi_{ww}(K_1,k_2')$ is the turbulence velocity wave number spectrum evaluated in the moving reference frame. Substituting Eq. (15) into Eq. (14) and performing the k_2' integration leads to

$$I^{\pm}(\mathbf{x},\omega) = \rho_0 M \int_{-\infty}^{\infty} \Phi_{ww}(K_1,k_2) \sum_{r=-\infty}^{\infty}\sum_{r'=-\infty}^{\infty} \times \mathrm{Re}\left\{ \begin{array}{l} \dfrac{\omega(-a\alpha_{r'}^{\pm *} + M_1(\omega + U_1\alpha_{r'}^{\pm *} + U_2\beta_{r'}))}{(\omega + U_1\alpha_r^{\pm} + U_2\beta_r)(\omega + U_1\alpha_{r'}^{\pm *} + U_2\beta_{r'})} \\ \times R_r^{\pm}(K_1,k_2) R_{r'}^{\pm *}(K_1,k_2) e^{i[(\alpha_r^{\pm} - \alpha_{r'}^{\pm *})x_1 + (\beta_r - \beta_{r'})x_2]} \end{array} \right\} dk_2. \tag{16}$$

The acoustic power per unit span can be obtained by integrating Eq. (16) in the x_2 direction over a distance of Bs.

Since the gap-wise wave numbers β_r and $\beta_{r'}$ are periodic over the distance Bs, this integral is of the form

$$\int_0^{Bs} e^{i(\beta_r-\beta_{r'})x_2}dx_2 = Bs\,\delta_{rr'}, \tag{17}$$

where the Kroneker delta function $\delta_{rr'}$ enables the r' summation in Eq. (16) to be eliminated. The acoustic power spectrum per unit span can therefore be expressed as

$$\mathcal{P}^{\pm}(\omega) = \rho_0 MBs \int_{-\infty}^{\infty} \Phi_{ww}(K_1,k_2) \sum_{r=-\infty}^{\infty} |R_r^{\pm}(K_1,k_2)|^2 \times \frac{\omega \mathrm{Re}\{-a\alpha_r^{\pm} + M_1(\omega + U_1\alpha_r^{\pm} + U_2\beta_r)\}}{|\omega + U_1\alpha_r^{\pm} + U_2\beta_r|^2} dk_2. \tag{18}$$

The periodicity of the turbulence in the x_2 direction (circumferential direction) allows the transverse Fourier integrals in k_2 to be converted to a Fourier series. Since the basic spatial period of the flow is the circumference Bs of the annulus under consideration, the wave number in the y_2 direction, as indicated by the relationship between the (x_1,x_2) and (y_1,y_2) coordinate systems in Fig. 1, must satisfy

$$k_{2,m} = \frac{2\pi m}{Bs\cos\theta} - K_1 \tan\theta, \tag{19}$$

where m is the vortical mode number in the circumferential direction. From Eq. (19), integration over k_2 at constant frequency (or K_1) requires that the elemental wave number $dk_{2,m}$ must be replaced by

$$dk_{2,m} \to \frac{2\pi\Delta m}{Bs\cos\theta}, \tag{20}$$

where $\Delta m = 1$. Thus, the k_2 integral may be written as a summation and Eq. (18) therefore becomes

$$\mathcal{P}^{\pm}(\omega) = \frac{2\pi\rho_0 M}{\cos\theta} \sum_{m=-\infty}^{\infty} \Phi_{ww}(K_1,k_{2,m}) \sum_{r=-\infty}^{\infty} |R_r^{\pm}(K_1,k_{2,m})|^2 \times \frac{\omega\,\mathrm{Re}\{-a\alpha_r^{\pm} + M_1(\omega + U_1\alpha_r^{\pm} + U_2\beta_r)}{|\omega + U_1\alpha_r^{\pm} + U_2\beta_r|^2}. \tag{21}$$

The radiated noise is therefore the sum of contributions from an infinite number of vortical modes, each of which scatters to produce an infinite number of acoustic modes. Equation (21) for the spectrum of sound power is not efficient for computation since $R_r^{\pm}$ appears inside the double summations of m and r. A transformation of the summation indices can be used to move $R_r^{\pm}$ out from the double summation into a single summation at the expense of moving the turbulence spectrum Φ_{ww} under the double summation. Overall, this is advantageous since Φ_{ww} will normally be computed from a simple algebraic expression, whereas $R_r^{\pm}$ requires another infinite summation of the so-called "cascade-waves" and the numerical computation of the upwash integral equation in Ref. 3. Since the basic spatial period of the flow is Bs, the acoustic wave number in the x_2 direction must satisfy

$$\beta_l = \frac{2\pi}{Bs} l, \tag{22}$$

where l is an arbitrary integer and denotes the order of the acoustic mode in the x_2 direction. Note that l is equivalent to the circumferential mode index m used in duct acoustic theory. Inserting Eqs. (19) and (22) into Eq. (5), the mth vortical wave number may be written in terms of the acoustic mode number l and the cascade scattering index r as

$$m = l + Br. \tag{23}$$

Equation (23) specifies the scattering rule for the generation of acoustic mode due to interaction of vortical modes with the cascade. Inserting Eq. (23) into Eq. (19) gives

$$k_{2,l+Br} = \frac{2\pi}{Bs\cos\theta}(l + Br) - K_1 \tan\theta. \tag{24}$$

By using Eq. (24), Eq. (21) can be rearranged as

$$\mathcal{P}^{\pm}(\omega) = \frac{2\pi\rho_0 M}{\cos\theta} \sum_{l=-\infty}^{\infty} Q_l^{\pm}(K_1) \sum_{r=-\infty}^{\infty} \Phi_{ww}(K_1,k_{2,l+Br}), \tag{25}$$

where $Q_l^{\pm}$ is a nondimensional modal power response function given by

$$Q_l^{\pm}(K_1) = |R_l^{\pm}(K_1,k_{2,\mathrm{mod}(l,B)})|^2 \times \frac{\omega\,\mathrm{Re}\{-a\alpha_l^{\pm} + M_1(\omega + U_1\alpha_l^{\pm} + U_2\beta_l)\}}{|\omega + U_1\alpha_l^{\pm} + U_2\beta_l|^2}. \tag{26}$$

The function, $\mathrm{mod}(l,B)$, denotes the remainder when the first argument is divided by the second argument. The modulus function emerges from the form of the cascade response function in Ref. 3, which has the property $K_{ji}^{-1}(\sigma_{l+Br})W_i = K_{ji}^{-1}(\sigma_{\mathrm{mod}(l,B)})W_i$. If we consider only the cut-on modal components in Eq. (25), the infinite summation over l in Eq. (25) becomes finite at a given frequency. In a subsonic flow, $W < a$, propagating modes corresponding to real values of $\alpha_r^{\pm}$ in Eq. (6), which occur over the range of β_l given by

$$\frac{M_2 - (1-M_1^2)^{1/2}}{1-M^2}\omega \leqslant a\beta_l \leqslant \frac{M_2 + (1-M_1^2)^{1/2}}{1-M^2}\omega. \tag{27}$$

We denote by $L_{\max}$ and $L_{\min}$ the maximum and minimum integers of the acoustic mode number l satisfying the upper and lower inequality of Eq. (27), respectively. These correspond to acoustic modes traveling in the direction of the swirl velocity U_2, and against it, respectively. Equation (25) can now be written as

$$\mathcal{P}^{\pm}(\omega) = \frac{2\pi\rho_0 M}{\cos\theta} \sum_{l=L_{\min}}^{L_{\max}} Q_l^{\pm}(K_1) \sum_{r=-\infty}^{\infty} \Phi_{ww}(K_1,k_{2,l+Br}), \tag{28}$$

where the range of r is chosen to ensure convergence. The corresponding sound power integrated over the frequency bandwidth $\omega_L \leqslant \omega \leqslant \omega_H$ can therefore be written as

$$\Pi^{\pm} = \frac{2\pi\rho_0 M}{\cos\theta} \int_{\omega_L}^{\omega_H} \sum_{l=L_{\min}}^{L_{\max}} Q_l^{\pm}(K_1) \sum_{r=-\infty}^{\infty} \Phi_{ww}(K_1, k_{2,l+Br}) d\omega. \tag{29}$$

The integration over ω in Eq. (29) is performed numerically in this paper.

C. Turbulence spectra

For simplicity we assume that the turbulence impinging on the cascade is homogeneous and isotropic. A suitable model for wave number PSD, which is consistent with these requirements, is the Liepmann spectrum $\Phi_{ww}(k_1,k_2,k_3)$ of the form,

$$\Phi_{ww}(k_1,k_2,k_3) = \frac{2\overline{w^2}\Lambda^3}{\pi^2} \frac{\Lambda^2(k_1^2+k_3^2)}{[1+\Lambda^2(k_1^2+k_2^2+k_3^2)]^3}, \tag{30}$$

where $\overline{w^2}$ is the mean square value of turbulence velocity in the direction normal to the chord and Λ is the turbulence integral length-scale. Integrating over k_3 gives the two-dimensional spectrum required in Eqs. (28) and (29) of the form,

$$\Phi_{ww}(k_1,k_2) = \frac{\overline{w^2}\Lambda^2}{4\pi} \frac{[1+\Lambda^2(4k_1^2+k_2^2)]}{[1+\Lambda^2(k_1^2+k_2^2)]^{5/2}}. \tag{31}$$

III. CHARACTERISTICS OF THE ACOUSTIC POWER SPECTRUM

In the following the above-developed theory to predict the acoustic power spectrum upstream and downstream of a two-dimensional flat-airfoil cascade interacting with homogeneous turbulence is now used to investigate the characteristics of the broadband sound field. These findings will be subsequently used to derive an expression for the acoustic power spectrum that is valid above a certain critical frequency. Unless otherwise stated, all the computations in this section were performed with a Mach number $M=0.5$, a stagger angle of $\theta=0°$, a turbulence intensity of $\overline{w^2}/W^2=4\times10^{-4}$, a turbulence integral length-scale of $\Lambda/c=0.05$, and a radius of $R/c=9/2\pi$ (i.e., $Bs/c=9$).

A. Critical frequency

Figure 2 presents the predicted acoustic power spectrum for the blade numbers of $B=4:4:24$ plotted against nondimensional frequency, $\omega/\Delta\omega_{\pm}$, where $\Delta\omega_{\pm}$ is the frequency separation between successive modal cut-on frequencies (note that $\Delta\omega_+=\Delta\omega_-$ for $\theta=0°$). The spectra contain a number of peaks occurring at integer values of $\omega/\Delta\omega_{\pm}$. These peaks can be divided into two categories. The first mostly occurs in the upstream spectra, at $\omega/\Delta\omega_{\pm}=nB$ ($n=1,2,3,\ldots$) and are characterized by narrow bandwidth and comparatively large amplitude. The other, smoother, peaks, occurring at the other integer values of $\omega/\Delta\omega_{\pm}$, except $\omega/\Delta\omega_{\pm}=nB$, have smaller amplitude and are closer together in frequency. These peaks occur at the cut-on frequencies of the cascade acoustic modes, defined by Eq. (27). The cut-on frequency of the lth cascade mode therefore occurs at

$$\omega_{l\pm} = l\Delta\omega_{\pm}, \tag{32}$$

where l is the acoustic mode number defined by the scattering rule $l=m-Br$ in Eq. (23) and $\Delta\omega_{\pm}$ is given by

$$\Delta\omega_{\pm} = \frac{1-M^2}{M_2 \pm (1-M_1^2)^{1/2}} \frac{2\pi a}{Bs}. \tag{33}$$

At frequencies below the cut-on frequency, the mode is cutoff and decays exponentially from the cascade. In this paper we refer to the lowest frequency of the large peak $l=B$ [i.e., plus sign in Eqs. (32) and (33)] as "the critical frequency," defined by

$$\omega_c = B\Delta\omega_+ = \frac{1-M^2}{M_2+(1-M_1^2)^{1/2}} \frac{2\pi a}{s}. \tag{34}$$

The significance of this frequency for cascade-turbulence interaction noise is twofold. First, the wavelength in the x_2 direction of the cascade acoustic mode, $l=B$, equals the blade spacing s. As the frequency increases above the critical frequency, the number of cut-on acoustic modes whose wavelength in the x_2 direction are less than the blade spacing s increases. These modes are therefore anticipated to have relatively weak interaction with the cascade. This property is employed in the next section in order to obtain a modal average value for the sound power. Second, it may be shown that at the critical frequency, all wave number components of turbulence excite propagating cascade modes, whereas below it, only some of the wave number components excite cut-on modes. Consequently, we will show that at frequencies below the critical frequency the acoustic field radiated from the cascade is sensitive to the interaction between neighboring blades. Above the critical frequency the acoustic field is relatively independent of interaction effects and therefore the radiated sound power from the different blades is additive. In order to demonstrate this phenomenon we compute the sound power versus blade number in a frequency band below the critical frequency for $B=24$ and in a frequency band above it. The results are shown in Fig. 3, nondimensionalized on $\rho_0 W^3 c$.

The results in Figs. 3(a) and 3(b) for the lower frequency band vary nonlinearly with the blade number B. In the higher frequency band, Figs. 3(c) and 3(d), however, the acoustic power is roughly proportional to B. The power at these high frequencies for the different blade numbers is therefore additive, suggesting that the interaction between blades is weak. The sensitivity of broadband noise radiation to cascade geometry therefore diminishes once the integration over all k_2 wave numbers is performed, as indicated in Eq. (18).

B. Approximate expression for the acoustic power spectrum

Here, we will derive an approximate expression for the acoustic power spectrum of Eq. (28) based on the findings obtained in Sec. III A. We now make the approximation in Eq. (28) that Φ_{ww} is a slowly varying function of k_2 such that the summation of Φ_{ww} over r is a weak function of l and may therefore be taken out from the summation over l. Correspondingly, we make the substitution,

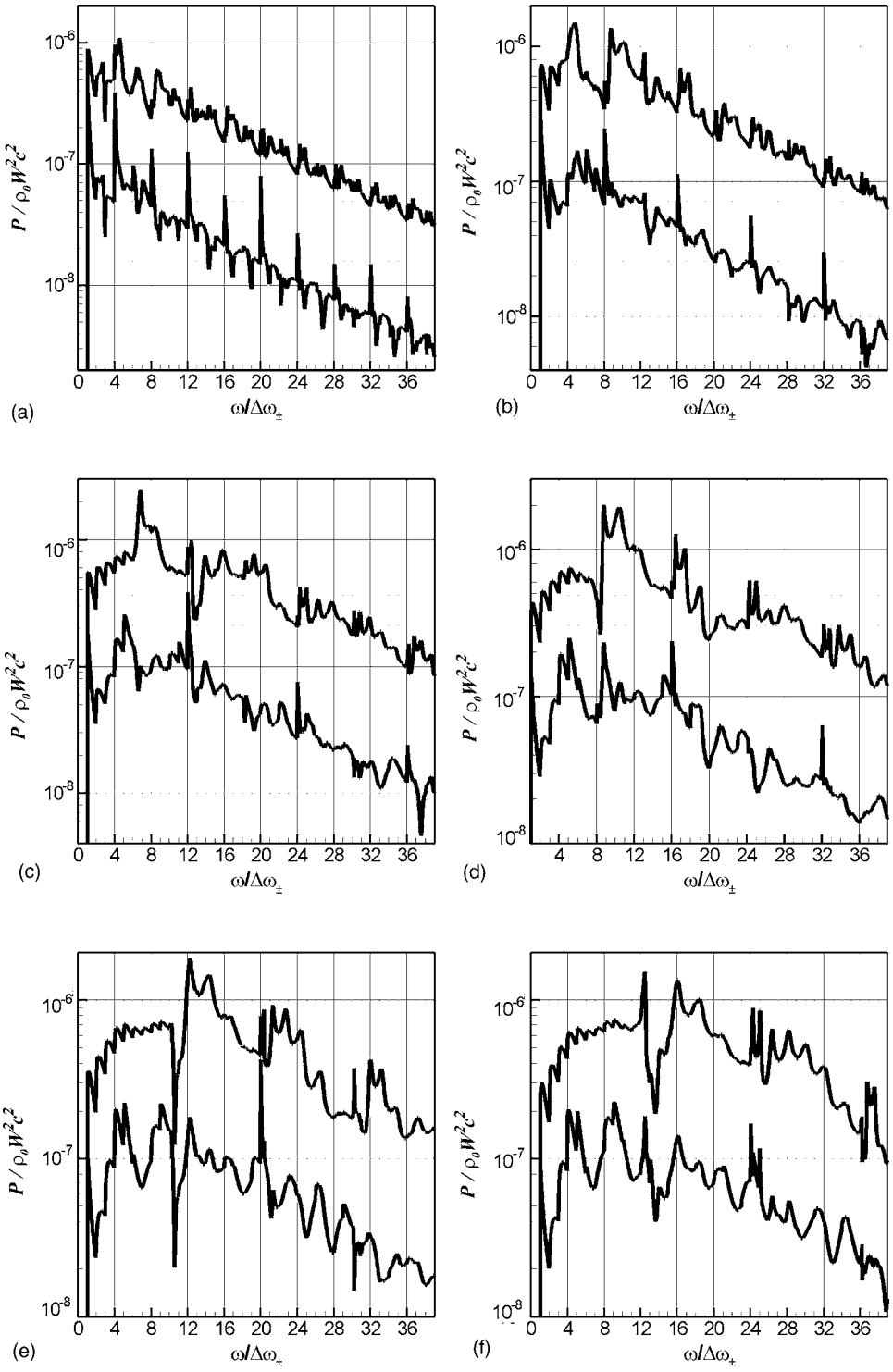

FIG. 2. Predicted spectrum of acoustic PSD: (a) $B=4$, (b) $B=8$, (c) $B=12$, (d) $B=16$, (e) $B=20$, and (f) $B=24$ where lower spectrum denotes the upstream spectrum and upper spectrum denotes the downstream spectrum.

$$\sum_{r=-\infty}^{\infty} \Phi_{ww}(K_1, k_{2,l+Br}) \approx \frac{1}{B} \sum_{m=-\infty}^{\infty} \Phi_{ww}(K_1, k_{2,m}), \tag{35}$$

such that the dependence on l can now be dropped. Equations (24) and (35) suggest that this is a valid approximation at high frequencies and integral length-scales small compared to the blade spacing, i.e., $\Lambda/s < 1$. Insertion of Eq. (35) into Eq. (28) leads to

$$\mathcal{P}^{\pm}(\omega) \approx \frac{2\pi\rho_0 M}{B\cos\theta} \sum_{m=-\infty}^{\infty} \Phi_{ww}(K_1, k_{2,m}) \sum_{l=L_{\min}}^{L_{\max}} Q_l^{\pm}(K_1) \quad \text{for } \omega > \omega_c. \tag{36}$$

This procedure has the effect of decoupling the turbulence wave number spectrum from the cascade response function. In order to verify the validity of Eq. (36), the power spectrum for $B=24$ and $\Lambda/c=0.1$ are computed using the exact expression of Eq. (28) and the approximate expression of Eq. (36). The error between the two predictions, calcu-

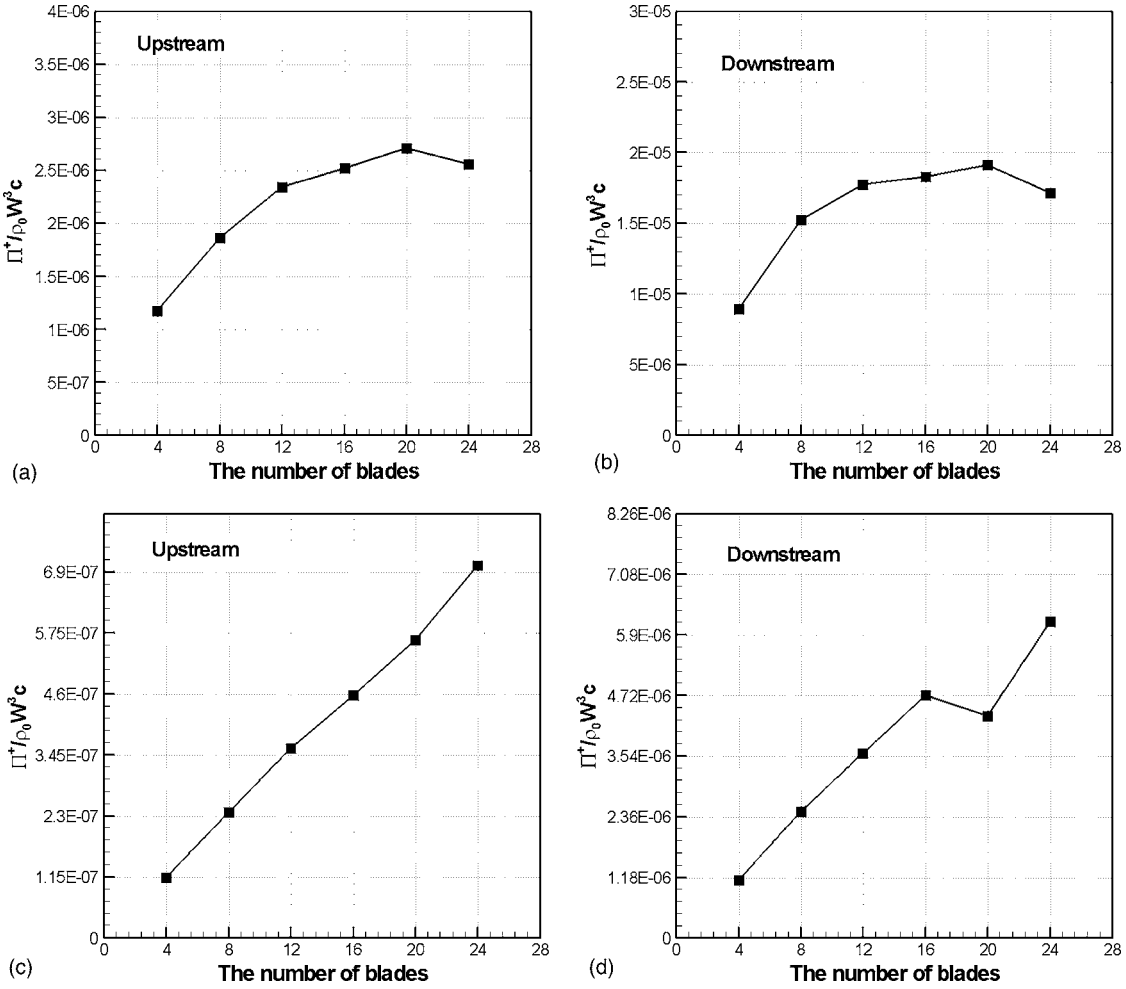

FIG. 3. Predicted band acoustic power with various blade number: (a) and (b) on lower bandwidth, $\omega<(\omega_c)_{B=24}$; (c) and (d) on higher bandwidth, $\omega>(\omega_c)_{B=24}$.

lated from $\epsilon=|(\mathcal{P}^{\pm}(\omega)-\tilde{\mathcal{P}}^{\pm}(\omega))/\mathcal{P}^{\pm}(\omega)|$ where the tilde denotes the approximate prediction, is plotted in Fig. 4. The error between the exact and approximate solutions is negligible at all frequencies, especially above the critical frequency where typical error is less than 1%. Figure 4 suggests that the error associated with Eq. (36) is negligible even at frequencies below the critical frequency. The requirement that the frequency range is above the critical frequency for Eq. (36) to be valid may therefore be relaxed.

We now introduce a further simplification to the sound power expression that is only valid at frequencies above the critical frequency. The basis for the technique involves replacing the frequency-dependence of $Q_l(K_1)$ in Eq. (36) by its high frequency asymptotic dependence. In order to ascertain this dependence, the function $\Sigma_{l=L_{\min}}^{L_{\max}} Q_l^{\pm}(K_1)$ appearing in Eq. (28) is computed for different blade numbers. The results are plotted in Fig. 5.

Also shown in these figures are the curves proportional to B^2/K_1, which provide a good fit to the exact behaviors at frequencies greater than their respective critical frequencies. Based on this goodness of fit, we write the high frequency response function of the cascade in the form,

$$\sum_{l=L_{\min}}^{L_{\max}} Q_l^{\pm}(K_1) \approx \frac{Bs\omega(1-M_1^2)^{1/2}}{\pi a(1-M^2)} \frac{aF^{\pm}(M,\theta)}{W\lambda^2(s/c)^2}, \tag{37}$$

where $F^{\pm}(M,\theta)$ is a nondimensional function that must only depend on M and θ. The argument leading to this formulation is presented in Appendix A.

The first term on the right-hand side of Eq. (37), as demonstrated by Eq. (27), approximates the number of cut-on modes. The second term therefore specifies the modal averaged acoustic power response, and is introduced such that the final form of Eq. (37) is proportional to B^2/K_1 while retaining the nondimensionality. Note that the chord length c cancels in the term, $\lambda^2(s/c)^2$. Insertion of Eq. (37) into Eq. (36) gives an approximation to the power spectral density of the form,

$$\mathcal{P}^{\pm}(\omega) \approx F^{\pm}(M,\theta)\frac{2\rho_0 MW(1-M_1^2)^{1/2}}{\omega s\cos\theta(1-M^2)} \sum_{m=-\infty}^{\infty} \Phi_{ww}(K_1,k_{2,m}) \quad \text{for } \omega \geqslant \omega_c. \tag{38}$$

Converting the $k_{2,m}$ summation into k_2 integration by the use of the inverse relation of Eq. (20) leads to

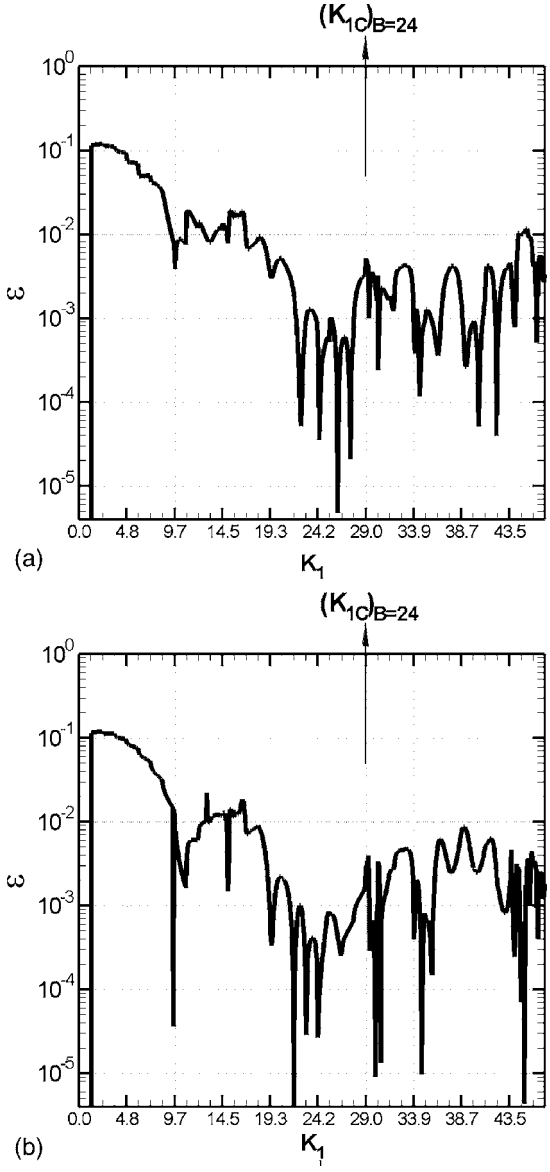

FIG. 4. Calculated error between the exact and approximate predictions for $B=24$ and $\Lambda=0.1$. Error is defined as $\epsilon=|(\mathcal{P}^{\pm}(\omega)-\tilde{\mathcal{P}}^{\pm}(\omega))/\mathcal{P}^{\pm}(\omega)|$ where a tilde denotes the prediction using the approximate equation, Eq. (36): (a) upstream and (b) downstream.

$$\mathcal{P}^{\pm}(\omega) \approx F^{\pm}(M,\theta)\frac{B\rho_0 M(1-M_1^2)^{1/2}}{\pi(1-M^2)}\frac{\Phi_{ww}(K_1)}{K_1} \quad \text{for } \omega \geqslant \omega_c, \tag{39}$$

where the turbulence one-dimensional (frequency) spectrum is given by $\Phi_{ww}(K_1)=\int_{-\infty}^{\infty}\Phi_{ww}(K_1,k_2)dk_2$. This formulation makes explicit that the acoustic power above the critical frequency is proportional to blade number and independent of the airfoil chord and solidity. In order to verify these dependencies from numerical predictions, we define a normalized acoustic power over the bandwidth $(\omega_c)_{B=4n} \leqslant \omega \leqslant (\omega_c)_{B=4n+4}$ in Fig. 2, given by

$$\bar{\Pi}_n^{\pm} = \frac{\int_{(\omega_c)_{B=4n}}^{(\omega_c)_{B=4n+4}}\mathcal{P}^{\pm}(\omega)d\omega}{\int_{(\omega_c)_{B=4n}}^{(\omega_c)_{B=4n+4}}\Phi_{ww}(K_1)/K_1 d\omega}. \tag{40}$$

If the approximate solution of Eq. (39) is valid, then $\bar{\Pi}_n \propto B$ for $B=4,\ldots,4n$ for the same values of M and θ, and the resultant curve of $\bar{\Pi}_n$ collapses onto a single curve proportional to the blade number. Equation (40) was computed using the same parameters used in Fig. 2, except with a solidity of $s/c=1$, i.e., $c=9/B$. In this computation, acoustic power was computed using the exact expression of Eq. (29). The result is plotted in Fig. 6. The normalized power is shown to be a function only of B, thereby confirming the validity of the approximate expression of Eq. (39) above the critical frequency.

The approximate power expression of Eq. (39) predicts explicitly that the acoustic power spectrum falls off as $\Phi_{ww}(K_1)/K_1$. The form of this function is obtained by integrating Eq. (31) over k_2 to give

$$\frac{\Phi_{ww}(K_1)}{K_1} = \frac{\overline{w^2}\Lambda}{2\pi}\frac{(1+3\Lambda^2K_1^2)}{K_1(1+\Lambda^2K_1^2)^2}, \tag{41}$$

which falls off as ω^{-3} as $\Lambda\omega/W(=\Lambda K_1)\to\infty$. Inserting Eq. (41) into Eq. (39) gives the spectrum of sound power per unit span at frequencies above the critical frequency as

$$\mathcal{P}^{\pm}(\omega) \approx F^{\pm}(M,\theta)\frac{B\rho_0\Lambda\overline{w^2}W}{2\pi^2\omega}\frac{M(1-M_1^2)^{1/2}}{(1-M^2)}\frac{(1+3\Lambda^2K_1^2)}{(1+\Lambda^2K_1^2)^2} \quad \text{for } \omega_c \geqslant \omega. \tag{42}$$

C. Characteristics of $F^{\pm}(M,\theta)$

In order to complete the approximate expression of Eq. (42), the cascade response function $F^{\pm}(M,\theta)$ defined by Eq. (37) must be known. In order to compute the dependence of $F^{\pm}(M,\theta)$ on M and θ, the acoustic power in frequency bands above critical frequency for $B=4$ were computed exactly using Eq. (28) for various values of M and θ, and their results equated to Eq. (42) to obtain $F^{\pm}(M,\theta)$. The function $F^{\pm}(M,\theta)$ is plotted in Fig. 7 over the range of values: $M=0.2:0.1:0.8$ and $\theta=15°:15°:75°$. Note that the values of $F^{\pm}$ computed from other values of B are within 0.1% for F^{+} and within 1% for F^{-}. The data were used to calculate the coefficients $a_{m,n}^{\pm}$ in a polynomial of least-squares fit, of the form $\hat{F}^{\pm}(M,\theta)=\Sigma_{m=0}^{2}\Sigma_{n=0}^{4}a_{m,n}^{\pm}\theta^n M^m$. The coefficients are tabulated in Appendix B. This function is plotted as the continuous curves in Fig. 7.

The accuracy of the approximate power expression of Eq. (42), combined with the results for $F^{\pm}(M,\theta)$ in Fig. 7, was verified by using it to compute the acoustic power spectral density of the exact results presented in Fig. 2. The results are shown in Fig. 8. Excellent agreement is obtained at frequencies above the critical frequencies. Below the critical frequency, however, agreement is poor, as expected.

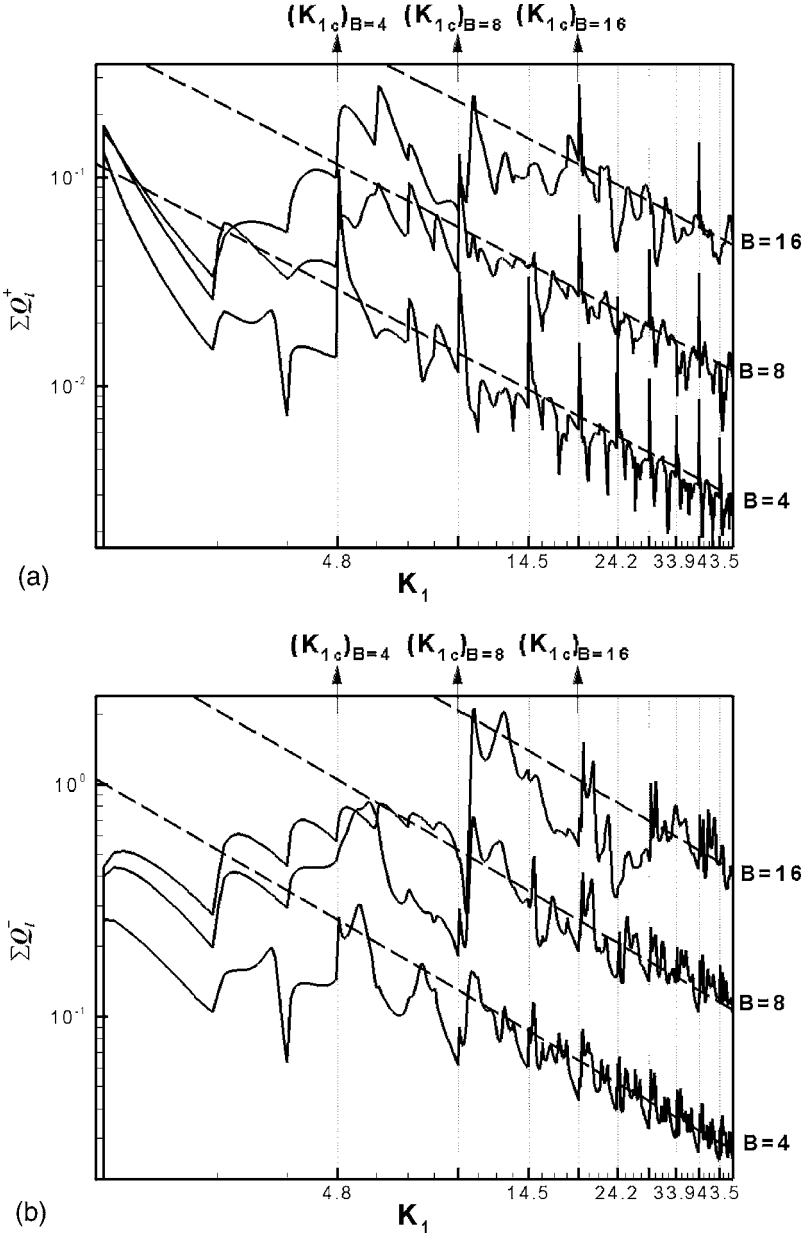

FIG. 5. Modal sum, $\Sigma_{l=L_{\min}}^{L_{\max}} Q_l^{\pm}(K_1)$, for different blade numbers and asymptotic lines. (—) Prediction results of $\Sigma_{l=L_{\min}}^{L_{\max}} Q_l^{\pm}(K_1)$ from Eq. (37) and (- - -) lines of const $\times B^2/K_1$: (a) upstream and (b) downstream.

IV. COMPARISON WITH MEASURED DATA

This section presents a comparison between the prediction and measured data for turbulence-cascade interaction noise. The spectra are expressed in decibels as a power level (PWL) defined as

$$\mathrm{PWL}^{\pm} = 10 \log_{10}\left(\frac{2\Pi^{\pm}\Delta R}{10^{-12}}\right), \tag{43}$$

where the factor of 2 is used to convert from a two-sided spectrum to a one-sided spectrum and ΔR denotes the width of the cascade in the spanwise direction.

Figure 9 shows a comparison between the sound power spectra predicted using the exact expression of Eq. (28), the approximate formulation of Eq. (42), and the experimental data obtained from a model test in a wind tunnel at NASA-Lewis.[11,13] The noise below 300 Hz was reported to be due to sources other than the fan. The stator is modeled by the two-dimensional geometry of Fig. 1, with a mean flow speed corresponding to that at the tip of the stator. The computations were performed for $M=0.5$, $B=45$, $s/c=0.8$, $\theta=30°$, $\bar{w}^2/W^2=4\times10^{-4}$, and $\Lambda/R=0.035$ at a radius of $R=0.80$ m. The calculation was performed with a frequency resolution of $\Delta\omega/W=\pi/40$ m^{-1} and for simplicity we assume that $\Delta R=R/2$. The turbulence length-scale and intensity were adjusted to provide a best match to the measured data.

Although the computation was carried out using two-dimensional theory, and the turbulence properties are represented simply by a single value of intensity and length scale, agreement overall is good. In particular, the rate of high-frequency roll-off closely matches that of the experimental data. Similar levels of agreement were obtained by Hanson[11,13] using three-dimensional theory with approxi-

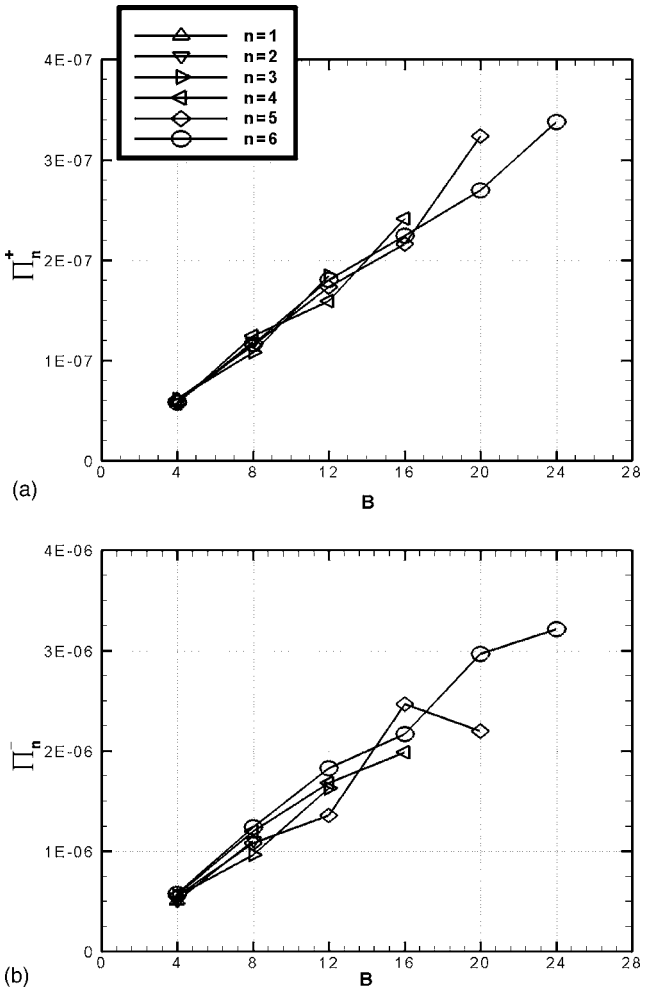

FIG. 6. Normalized characteristic band acoustic power: (a) upstream and (b) downstream.

mately the same values of Λ and $\bar{w}^2$. The use of two-dimensional theory to give comparable results with the three-dimensional theory suggests that three-dimensional effects, such as the contribution from oblique gusts, are comparatively weak.

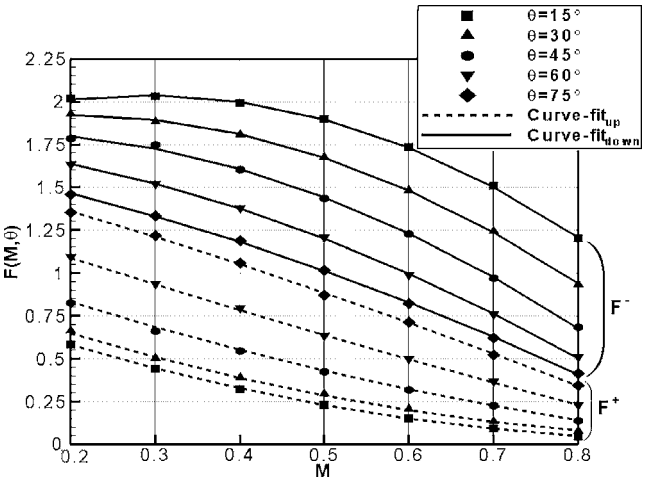

FIG. 7. The dependence of the function $F^{\pm}$ on Mach numbers and stagger angles for $B=4$. Symbols denote the calculation and lines denote a polynominal of least-squares fit.

V. PARAMETRIC STUDY

For the parametric study presented in the following, a baseline case is chosen to correspond to that in Sec. IV, except that the vane count was changed to 30. Vane count is a major consideration for tonal noise since the use of large vane numbers leads to cutoff of the first blade passing frequency. In designing stators, there is usually a preferred solidity for aerodynamic efficiency purpose, but some variability in the vane count is permitted.

Figure 10 shows the variation of power levels, in one-third octave band frequencies, for $B=15,30$, and 60 while keeping solidity, and hence the wetted area, constant. The solid lines represent the predictions obtained using the approximate expression of Eq. (42). Excellent agreement between the exact and approximate predictions is observed at frequencies above the critical frequencies of 660.9, 1321.8, and 2643.6 Hz for $B=30,45$, and 60, respectively. The power above the critical frequency is observed to be proportional to B, as predicted explicitly by Eq. (42). The poor agreement between the exact and approximate calculations below the critical frequencies is due to interactions between neighboring vanes. The center frequency of the "hump" in the spectra is also observed to be proportional to B. Figure 10 suggests that below the critical frequency there exists a saturation blade number, above which the overall acoustic power ceases to increase.

Figure 11 shows the power spectrum for the stagger angles of 15° and 45° for $B=30$. Again, excellent agreement is obtained between the exact and approximate predictions above the critical frequency. Due to convection effects, the high frequency upstream power spectrum increases with increasing stagger angle and decreases for the downstream power spectrum. However, the effect of stagger angle on the downstream spectrum is generally small, particularly at high frequencies.

Figure 12 shows the variation of power spectra for the three gap-chord ratios of $s/c=0.4$, 0.8, and 1.2 for $B=30$ and $\theta=30°$. The approximate expression of Eq. (42) predicts that the sound power is independent of gap-chord ratio (or solidity) above the critical frequency, as confirmed by the exact calculation. Chord length therefore has little effect on sound radiation, especially at high frequencies.

In order to investigate the effect of flow speed Mach number on broadband noise generation, acoustic power spectra were computed for Mach numbers of $M=0.4$, 0.5, and 0.6 using the exact and approximate expressions. The results are plotted in Fig. 13. Again, close agreement is obtained above the critical frequency.

A similar parametric study was carried out by Hanson[11,13] over a range of mean-flow and cascade parameters similar to those above. Overall trends with the various parameters obtained here closely match those predicted by Hanson,[11,13] using a three-dimensional theory. The significant difference in our study is that these trends are predicted

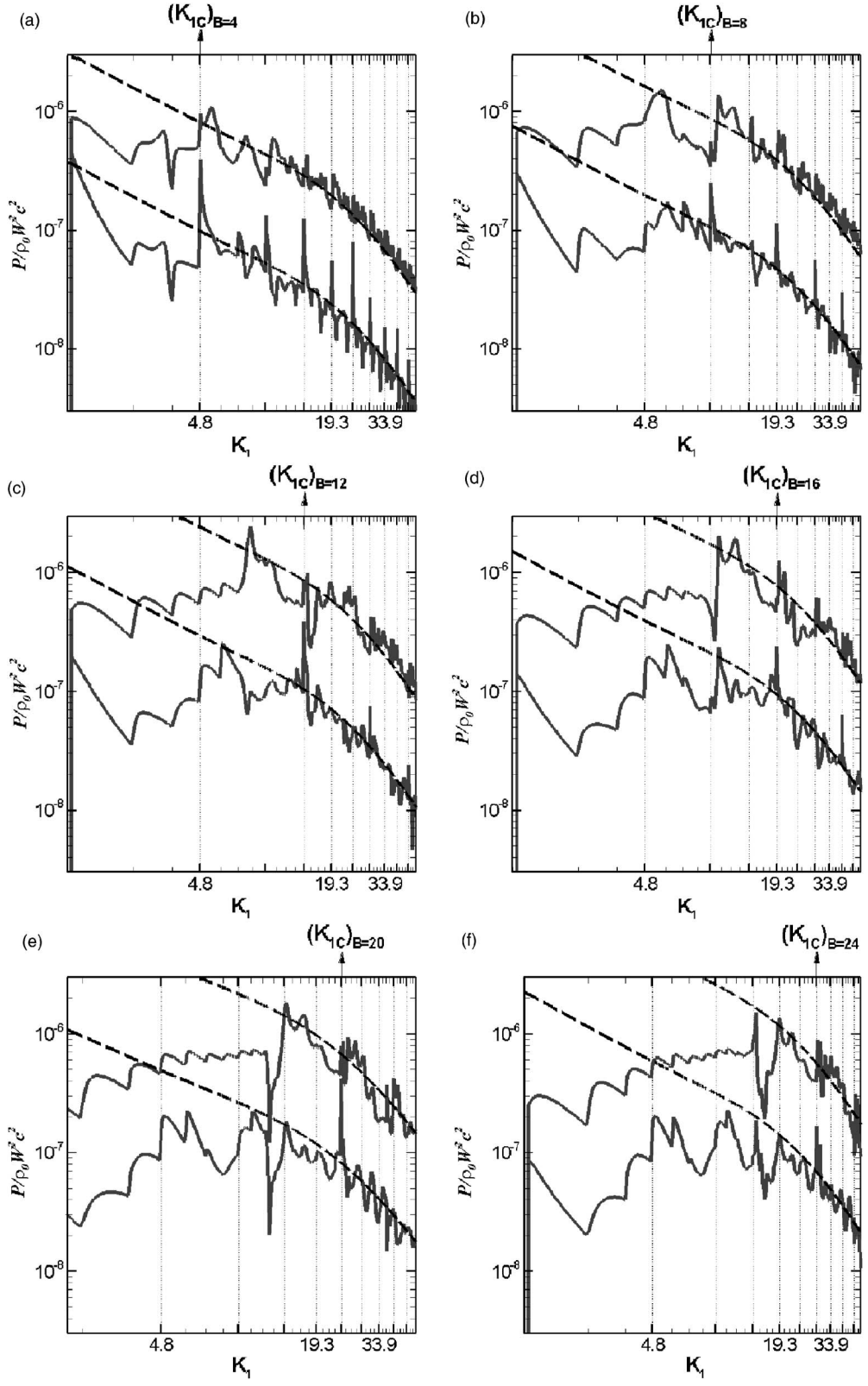

FIG. 8. Comparison of power spectral density between the exact and approximate predictions [exact solutions (—), approximate solutions (- - -)]: (a) $B=4$, (b) $B=8$, (c) $B=12$, (d) $B=16$, (e) $B=20$, and (f) $B=24$.

explicitly by the approximate high frequency result of Eq. (42).

VI. CONCLUSION

The power spectrum of the upstream and downstream sound field due to an isotropic frozen turbulent gust impinging on a cascade of flat-plate airfoils has been computed. The theory has been developed using an analytic formulation of the two-dimensional response by a cascade of flat plates derived from the theory due to Smith[3] and the LINSUB computer code by Whitehead.[4] It is found that the acoustic power spectrum can be categorized into two distinct frequency regions,

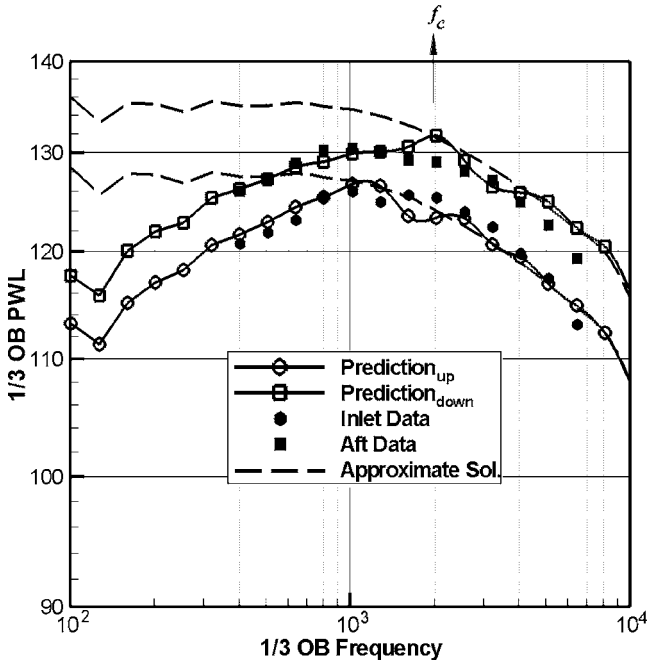

FIG. 9. Comparison of theoretical prediction with measured noise spectra for model data.

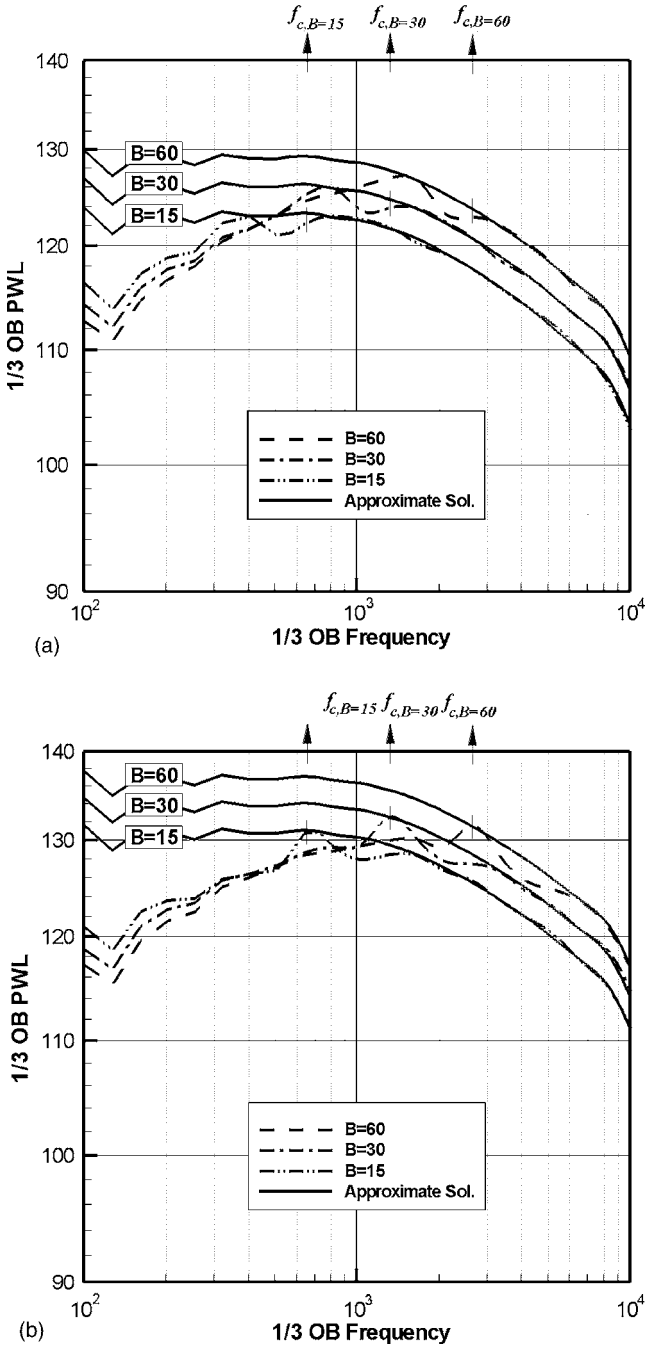

FIG. 10. Variation of acoustic power spectrum with blade number, B; solid lines denote approximate predictions and the other lines exact predictions; vertical line "|" denotes the location of critical frequency: (a) upstream and (b) downstream.

which are separated by a critical frequency. This critical frequency corresponds to the cutoff frequency of the mode $l=B$, i.e., when the gap-wise wavelength equals the blade space. Below this frequency, only some spectral components of turbulence excite cuton acoustic modes. Above the critical frequency, all wave number components of turbulence contribute to cut-on acoustic modes and interaction between acoustic waves radiated from each blade is weak. The blades therefore radiate incoherently and their sound powers are additive. Based on this finding, a simplified, cascade-response/turbulence-spectrum decoupled expression has been derived for the acoustic power spectrum at frequencies above the critical frequency. This expression explicitly predicts that the acoustic power above the critical frequency is proportional to the blade number, independent of the blade chord, and varies with frequencies as $\Phi_{ww}(\omega/W)/\omega$, where $\Phi_{ww}(\omega/W)$ is the wave number spectrum of the turbulence velocity. The theory was utilized to perform a parametric study which shows that overall predictions and trend closely match those predicted by Hanson[11,13] obtained using a three-dimensional theory. This result suggests that three-dimensional effects such as the contribution to the power from oblique gusts are comparatively weak. Through the comparison between experimental data and predictions using the exact and approximated expressions, the approximate expression is shown to provide a highly efficient means of computing the power spectrum at high frequencies above the critical frequency, which for realistic engine parameters, corresponds to about 1 kHz.

Future work is aimed at extending the approximate formula to the prediction of broadband noise due to three-dimensional excitation by inhomogeneous turbulence impinging on a rectilinear cascade of flat-plate airfoils.

ACKNOWLEDGMENTS

This work was supported by the Post-doctoral Fellowship Program of Korea Science & Engineering Foundation (KOSEF) and by the International Cooperation Research Program of the Ministry of Science & Technology. The authors would also like to thank Vincent Jurdic for detecting an error in an earlier draft of this paper.

Nomenclature

a = sound speed

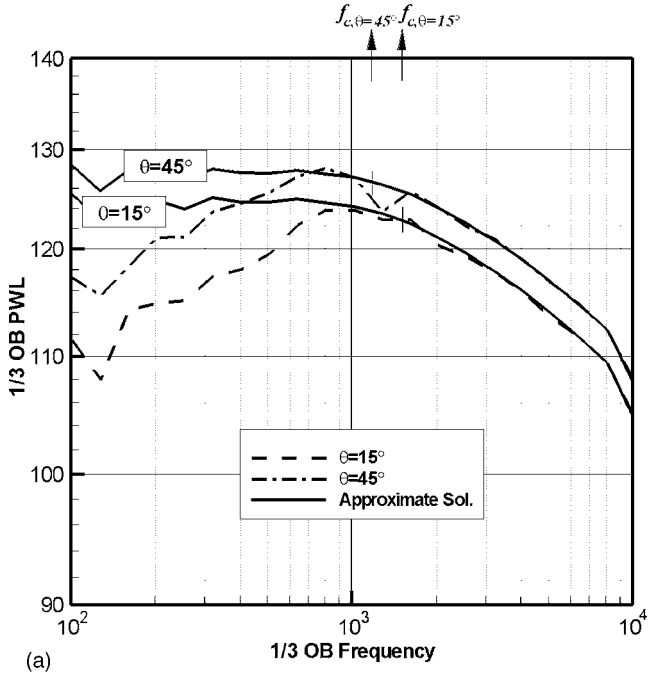

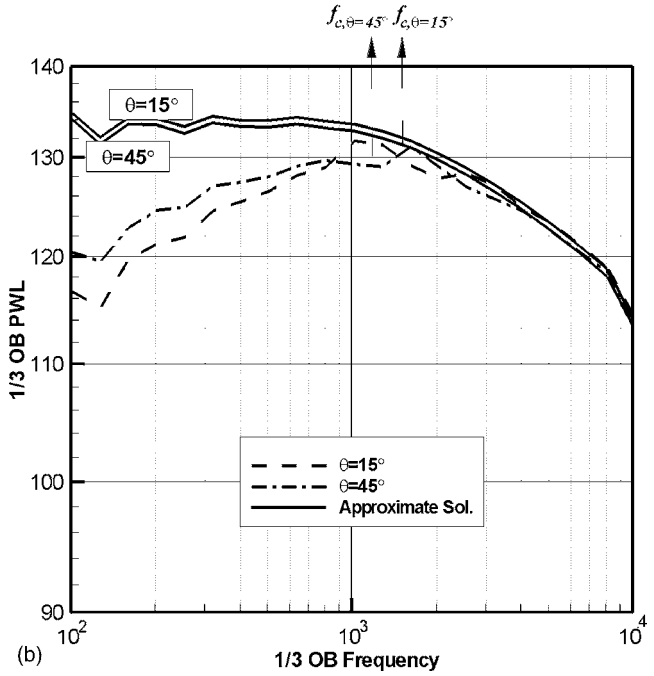

FIG. 11. Variation of acoustic power spectrum with stagger angle, θ; solid lines denote approximate predictions and the other lines exact predictions; vertical line "|" denotes the location of critical frequency: (a) upstream and (b) downstream.

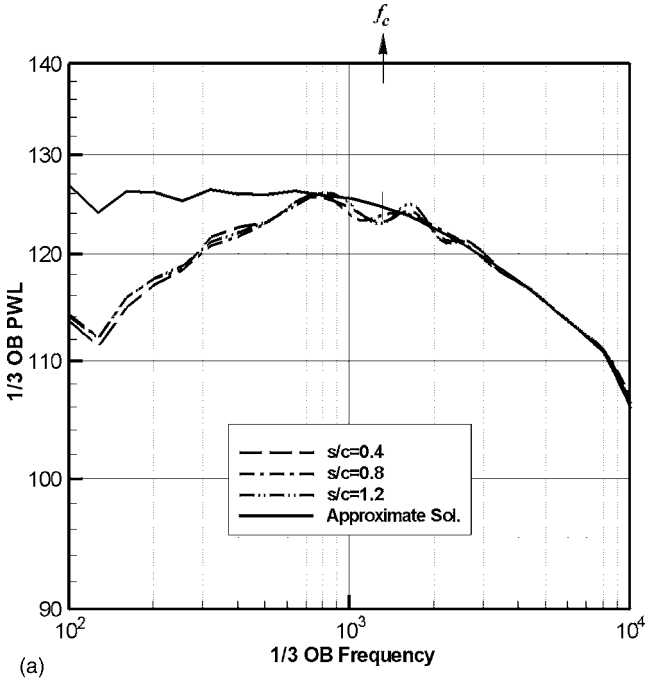

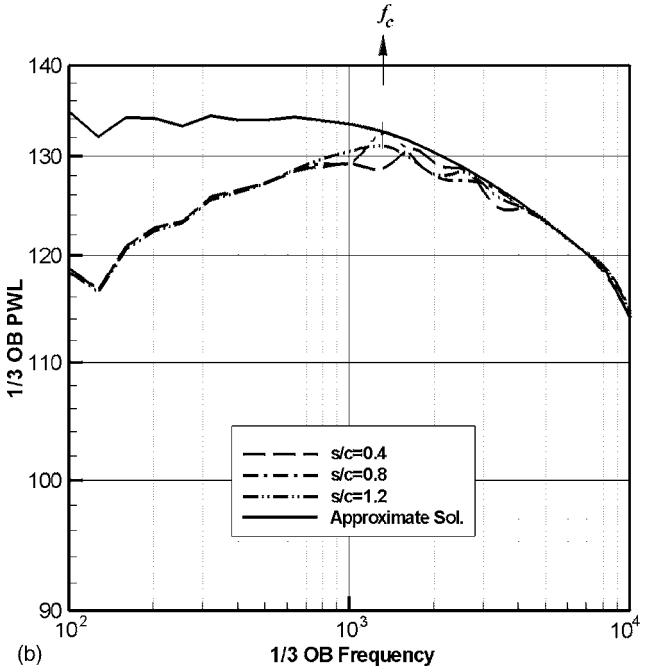

FIG. 12. Variation of acoustic power spectrum with gap-chord ratio s/c (or reciprocal of solidity); solid lines denote approximate predictions and the other lines exact predictions; vertical line "|" denotes the location of critical frequency: (a) upstream and (b) downstream.

B = the number of airfoils in a cascade
c = airfoil chord length
l = acoustic mode number in the gap-wise direction
m = vortical mode number in the gap-wise direction
M = Mach number of mean-flow
M_1 = Mach number in the axial direction, $M \cos \theta$
M_2 = Mach number in the gap-wise direction, $M \sin \theta$
k_i = wave number of ingested turbulence gust in Cartesian coordinate system
K_1 = ω/W
p = pressure perturbation
r = scattering index for a cascade of airfoils
R = radius or cascade response function
s = blade spacing or entropy
t = time
u_i = velocity perturbation in x_i direction
U_i = mean velocity in x_i direction
w = upwash velocity perturbation

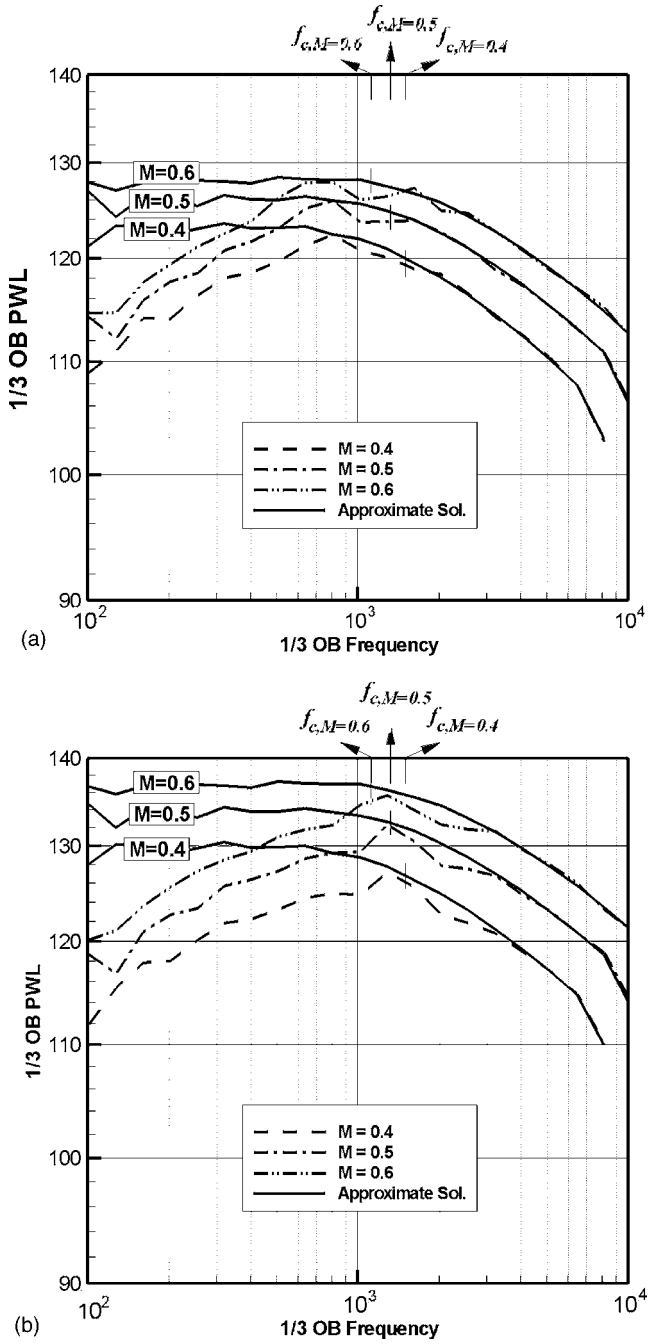

FIG. 13. Variation of acoustic power spectrum with Mach number, M; solid lines denote approximate predictions and the other lines exact predictions; vertical line "|" denotes the location of critical frequency: (a) upstream and (b) downstream.

W = mean-flow speed, $\sqrt{U_1^2+U_2^2}$
x_i = Cartesian duct coordinate system, Fig. 1
y_i = Cartesian cascade-fixed coordinate system, Fig. 1
z = coordinate measured in direction of airfoil chord, Fig. 1
α = wave number of the generated disturbance in the axial direction
β = wave number of the generated disturbance in the gap-wise direction
Γ = vortex strength
Φ_{ww} = turbulence spectrum
θ = stagger angle, $\tan^{-1}(U_2/U_1)$
λ = reduced frequency $\omega c/W$
ρ = density perturbation
ρ_0 = mean-stream density
σ = interblade phase angle
ω = angular frequency
PSD = power spectral density

Superscripts

$+$ = upstream running acoustic wave
$-$ = downstream running acoustic wave
$\wedge$ = convected vorticity wave

APPENDIX A: ARGUMENT FOR THE ANALYTIC FORM OF EQ. (37)

This appendix presents the reasoning for Eq. (37), which is reproduced in the following, for the modal power response function summed over all propagating modes,

$$\sum_{l=L_{\min}}^{L_{\max}} Q_l^{\pm}(K_1) \approx \frac{Bs\omega(1-M_1^2)^{1/2}}{\pi a(1-M^2)} \frac{aF^{\pm}(M,\theta)}{W\lambda^2(s/c)^2}.$$

The form of the right-hand side of this equation may be derived from the following observations:

i. From Sec. III A, the band acoustic power above the critical frequency is proportional to B.
ii. From Eq. (35), the contribution of the wave number spectrum of the turbulence to the acoustic power varies as B^{-1}.
iii. Observations i and ii suggest that the power term, $\Sigma Q_l^{\pm}(K_1)$, in Eq. (28) must be proportional to B^2.
iv. From Fig. 5, $\Sigma Q_l^{\pm}(K_1)$ is inversely proportional to K_1.

Based on i–iv, dimensional analysis was used to derive Eq. (37) for $\Sigma Q_l^{\pm}(K_1)$ to give the desired dependence of B^2/K_1. The first term on the right-hand side of Eq. (37) represents the number of cut-on modes and is proportional to K_1 ($Bs=2\pi R$, i.e., constant). The second term must therefore be proportional to B^2/K_1^2. This second term there has the interpretation as the modal averaged cascade response function of Smith in Ref. 3, which is uniquely defined by the gap-chord ratio s/c, stagger angle θ, Mach number M, and reduced frequency λ. Note that, unlike for harmonic gusts, the phase angle σ has no physical meaning for turbulent gusts and can therefore be neglected as an input parameter in the dimensional analysis. We assume the form, $(s/c)^{\alpha}\lambda^{\eta}F^{\pm}(M,\theta)$ for this second term. First, we must have $\eta=-2$ and $\alpha=-2$ in order to give the required frequency dependence of K_1^{-2} and B dependence of B^2 identified in iii and iv, since s^{-1} is proportional to B ($B=2\pi R/s$). The precise dependence on M and θ cannot be determined from the observations i–iv, and so their dependence is incorporated into the function $F^{\pm}(M,\theta)$. The term of a/W in Eq. (37) is introduced to cancel the same term in the first term on the right-hand side. This procedure leads to the final form of Eq. (37).

TABLE I. The calculated coefficients, $a^{\pm}_{n,m}$ in the polynomial of least-squares fit for the function $F^{\pm}$: $\hat{F}^{\pm}(M,\theta)=\sum_{m=0}^{2}\sum_{n=0}^{4}a^{\pm}_{m,n}\theta^n M^m$.

		m		
n		0	1	2
0	$a^{+}_{0,m}$	1.069 02	−2.072 80	1.008 61
	$a^{-}_{0,m}$	1.507 91	3.955 33	−5.245 09
1	$a^{+}_{1,m}$	−1.080 14	1.290 47	−0.064 344 3
	$a^{-}_{1,m}$	1.696 50	−12.853 7	13.722 7
2	$a^{+}_{2,m}$	2.090 42	−2.119 89	−0.174 021
	$a^{-}_{2,m}$	−3.357 71	23.786 6	−29.140 3
3	$a^{+}_{3,m}$	−0.712 208	1.205 46	−0.451 791
	$a^{-}_{3,m}$	2.886 37	−22.734 3	28.229 1
4	$a^{+}_{4,m}$	0	0	0
	$a^{-}_{4,m}$	−0.944 190	7.565 42	−9.185 14

APPENDIX B: A POLYNOMIAL OF LEAST-SQUARES FIT FOR $F^{\pm}(M,\Theta)$—TABLE I

[1]S. Kaji and T. Okazaki, "Propagation of sound waves through a blade row II. Analysis based on the acceleration potential method," J. Sound Vib. **11**, 355–375 (1970).

[2]S. Kaji and T. Okazaki, "Generation of sound by a rotor stator interaction," J. Sound Vib. **13**, 281–307 (1970).

[3]S. N. Smith, "Discrete frequency sound generation in axial flow turbomachines," Reports and Memoranda No. 3709, Aeronautical Research Control Council, London, 1972.

[4]D. S. Whitehead, "Classical two-dimensional methods," in *Unsteady Turbomachinery Aerodynamics* (AGARD-AG-298), edited by M. F. Platzer and F. O. Carta, AGARD Manual on Aeroelasticity in Axial Flow Turbomachines, Vol. 1 (Neuilly sur Seine, France, 1987), Chap. 3.

[5]R. Mani and G. Hovray, "Sound transmission through blade rows," J. Sound Vib. **12**, 59–83 (1971).

[6]W. Koch, "On transmission of sound through a blade row," J. Sound Vib. **18**, 111–128 (1971).

[7]N. Peake, "The scattering of vorticity waves by an infinite cascade of flat plates in subsonic flow," Wave Motion **18**, 255–271 (1993).

[8]N. Peake, "The interaction between a high frequency gust and a blade row," J. Fluid Mech. **241**, 261–289 (1992).

[9]N. Peake and E. J. Kerschen, "Uniform asymptotic approximation for high frequency unsteady cascade flow," Proc. R. Soc. London London **449**, 177–186 (1995).

[10]S. A. L. Glegg, "The response of a swept blade row to a three-dimensional gust," J. Sound Vib. **227**, 29–64 (1999).

[11]D. B. Hanson and K. P. Horan, "Turbulence/cascade interaction: Spectra of inflow, cascade response, and noise," AIAA-98-2319, 1998.

[12]D. B. Hanson, "Influence of lean and sweep on noise of cascades with turbulent inflow," AIAA-99-1863, 1999.

[13]D. B. Hanson, "Theory for broadband noise of rotor and stator cascades with inhomogeneous inflow turbulence including effects of lean and sweep," NASA Contract Rep. NASA CR **2001**-210762 (2001).

[14]I. Evers and N. Peake, "On sound generation by the interaction between turbulence and a cascade of airfoils with non-uniform mean flow," J. Fluid Mech. **463**, 25–52 (2002).

[15]M. E. Goldstein, *Aeroacoustics* (McGraw-Hill, New York, 1976).

[16]R. K. Amiet, "Acoustic radiation from an airfoil in a turbulent stream," J. Sound Vib. **41**, 407–420 (1975).